Check for updates

Geophysical Research Letters

RESEARCH LETTER
10.1029/2021GL092568

Key Points:

- Long-term changes in the delay of the breakdown of the Southern Hemisphere stratospheric polar vortex can be largely explained by a linear response to ozone-depleting substances and to global warming
- The tug-of-war between ozone recovery and global warming manifests itself in the stratospheric vortex breakdown delay and propagates to the troposphere
- The uncertainty in future changes in regional precipitation in the Southern Hemisphere is subject to the combined effects of the uncertainty in tropical warming and in the vortex breakdown delay

Supporting Information:

Supporting Information may be found in the online version of this article.

Correspondence to:

T. G. Shepherd,
theodore.shepherd@reading.ac.uk

Citation:

Mindlin, J., Shepherd, T. G., Vera, C., & Osman, M. (2021). Combined effects of global warming and ozone depletion/recovery on Southern Hemisphere atmospheric circulation and regional precipitation. *Geophysical Research Letters*, *48*, e2021GL092568. https://doi.org/10.1029/2021GL092568

Received 18 JAN 2021
Accepted 22 MAY 2021

© 2021. The Authors.
This is an open access article under the terms of the Creative Commons Attribution License, which permits use, distribution and reproduction in any medium, provided the original work is properly cited.

Combined Effects of Global Warming and Ozone Depletion/Recovery on Southern Hemisphere Atmospheric Circulation and Regional Precipitation

Julia Mindlin[1,2,3], Theodore G. Shepherd[4], Carolina Vera[1,2,3], and Marisol Osman[1,2,3]

[1]Centro de Investigaciones del Mar y la Atmósfera, Consejo Nacional de Investigaciones Científicas y Técnicas, Universidad Nacional de Buenos Aires, Buenos Aires, Argentina, [2]Departamento de Ciencias de la Atmósfera y los Océanos, Facultad de Ciencias Exactas y Naturales, Universidad de Buenos Aires, Buenos Aires, Argentina, [3]Instituto Franco Argentino Sobre Estudios de Clima y sus Impactos (IFAECI-UMI3351), Centre National de la Recherche Scientifique, Buenos Aires, Argentina, [4]Department of Meteorology, University of Reading, Reading, UK

Abstract Ozone depletion led to a positive trend in the summertime Southern Annular Mode (SAM) during the last decades of the 20th century. During the present century, global warming (GW) is expected to contribute to a positive SAM trend while ozone recovery is expected to act in the opposite direction. Here, Southern Hemisphere (SH) circulation and regional precipitation change are studied with a methodology that separates the effects from GW and ozone depletion/recovery. Our results show that a "tug-of-war" between ozone and GW occurs in the summertime stratosphere, propagating to the troposphere where it is manifest in the SAM. However, at the regional scale this "tug-of-war" is not as relevant as the combined effects of other remote drivers of circulation change, which force different kinds of precipitation changes in the SH. For regional precipitation changes, the uncertainty in future circulation change is as important as the uncertainty in the GW level.

Plain Language Summary In the Southern Hemisphere, both ozone depletion and global warming have influenced climate in the past decades. Ozone recovery is expected to reverse the influence of ozone depletion, but the influence of global warming is expected to grow. Here, we investigate the combined effects of these anthropogenic forcings through the second half of the 20th century and the entire 21st century, quantifying their influence on stratospheric and tropospheric circulation and on regional precipitation changes. We find that the summertime stratosphere is affected by a "tug-of-war" between these two forcings, and that its effect propagates downward to the tropospheric circulation. On the other hand, summer precipitation in the land areas of the SH that are expected to experience large effects of climate change are not strongly affected by this "tug-of-war," but are instead influenced by the effects of both stratospheric and tropical tropospheric changes.

1. Introduction

Both observational (Randel & Wu, 1999; Young et al., 2013) and modeling (Arblaster & Meehl, 2006; McLandress et al., 2010; Stolarski et al., 2010) studies have shown a clear cooling in the Antarctic lower stratosphere in late-spring during the last decades of the 20th century associated with ozone depletion. As a consequence, the stratospheric polar vortex (SPV) has strengthened and the breakdown date delayed by about 2 weeks (McLandress et al., 2010; Waugh et al., 1999). This vortex strengthening propagates downward, intensifying and shifting poleward the westerly winds, as manifested in the Southern Annular Mode (SAM) (Gillett & Thompson, 2003; Son et al., 2010; Thompson & Solomon, 2002). Global warming is expected to lead to similar changes in the westerlies (Kushner et al., 2001), however, ozone recovery can be expected to act in the opposite sense (Son et al., 2010). How this "tug-of-war" on the SAM evolves during the 21st century will have significant impacts for Southern Hemisphere (SH) regional climate.

It has been recently shown that the poleward shift of the westerlies and positive SAM trend induced by global warming is in part induced by a delayed SPV breakdown (Ceppi & Shepherd, 2019; Mindlin et al., 2020). Mindlin et al. (2020) showed that two principal drivers of the effect of global warming on summer SH circulation were tropical upper-tropospheric warming (leading to a strengthening of the westerlies) and the delayed breakdown of the SPV (leading to a poleward shift of the westerlies), both contributing to a more

positive phase of the SAM. However, because of the different nature of these zonal wind changes, the two drivers have different effects on regional precipitation change, despite both having a positive effect on the SAM index. This suggests that a "tug-of-war" between tropospheric and stratospheric drivers might be an oversimplification, since the effect of these two remote drivers on tropospheric circulation and regional precipitation is not the same. On the other hand, a "tug-of-war" could occur through the stratosphere, where global warming and ozone recovery are expected to induce opposite changes on the SPV breakdown during the 21st century.

The goal of this study is to extend the approach of Mindlin et al. (2020) to include the effect of both global warming and ozone depletion/recovery on the SPV breakdown, and thereby on regional SH climate, testing the hypothesis of the "tug-of-war" occurring in the stratosphere. We do this by taking into account both drivers of the SPV breakdown delay together with tropical upper-tropospheric warming, and constructing time-dependent storylines for SH circulation and regional precipitation changes associated with different responses of the remote drivers to anthropogenic forcings. With this, we can describe the spread in the Coupled Model Intercomparison Project Phase 6 (CMIP6) models in a physically interpretable way.

2. Data and Methods

We used output from 29 models of the CMIP6 (Eyring et al., 2016) combining the period 1950–2014 with the period 2015–2099 from the historical and SSP5-8.5 experiments (Table S1).

To investigate the combined effects of greenhouse gases and ozone depleting substances in the stratosphere we performed a time series analysis, regressing the time-evolution of the vortex breakdown delay (VB_{delay}) simulated by each individual model onto global warming (GW) and equivalent effective stratospheric chlorine (EESC) at the pole (Newman et al., 2007). These two regressors represent the two anthropogenic forcings. The vortex breakdown (VB) occurs in the late-spring/early summer season (ONDJ), therefore the first and last months of our time series are October 1950 and January 2099, making a total of 149 years. For models that have more than one ensemble member available (Table S1) we created an ensemble from all possible combinations of both experiments, to reduce the uncertainty in the inter-annual variability through the ensemble mean. Results are shown for the ensemble mean of these combinations.

We computed the VB date as that by which the zonal winds at 50 hPa between 50°S and 60°S slow below 19 ms^{-1} within the ONDJF season. The VB_{delay} is defined as the difference of this date from its climatology in 1950–1969. Previous studies have used 10 ms^{-1} as threshold and Mindlin et al. (2020) used 15 ms^{-1} because in some CMIP5 models the vortex strength does not decline below this threshold; in CMIP6 models the vortex is even stronger, and 19 ms^{-1} was the lowest applicable threshold. However, it has been shown that the large-scale climate responses are insensitive to the exact definition of VB (Ceppi & Shepherd, 2019). We evaluated the GW index for each model as the annual global mean surface temperature (tas) change with respect to the 1950–1969 climatology. The midlatitude EESC time-series was taken from WMO (2014) and used to construct the polar EESC time-series following Newman et al. (2007).

In the second part of the study, we quantified how the stratospheric changes studied in the first part combine with tropospheric drivers to determine SH circulation and regional precipitation changes, and represent the combined effects through storylines. Each storyline is a physically plausible pathway for global change (Shepherd, 2019). To articulate the circulation and regional precipitation changes under each storyline we linearly combined the sea level pressure (*slp*) and precipitation (*pr*) sensitivity to remote drivers, each multiplied by the time series of the corresponding anthropogenic forcing (GW and EESC). We used a regression across models to determine the sensitivity of slp and pr to the GW-induced VB_{delay} and tropical warming (TW), the latter evaluated as the long-term change in temperature (*ta*) at 250 hPa zonally averaged between 15°S and 15°N (ΔT_{trop}) divided by the global surface temperature change (ΔT). Here Δ indicates the difference between 2070–2099 in the SSP5-8.5 experiment and 1950–1979 in the historical experiment. All averages were area-weighted. To determine the sensitivity of slp and pr to the EESC-induced VB_{delay}, we instead used the difference between the 1991–2020 and 1950–1979 periods, in order to maximize the signal, while controlling for the GW-induced changes over this period. With this framework, we allowed for VB delays forced by GW and EESC to drive different changes in the fields. More details are provided further below, as well as in the Supporting Information S1.

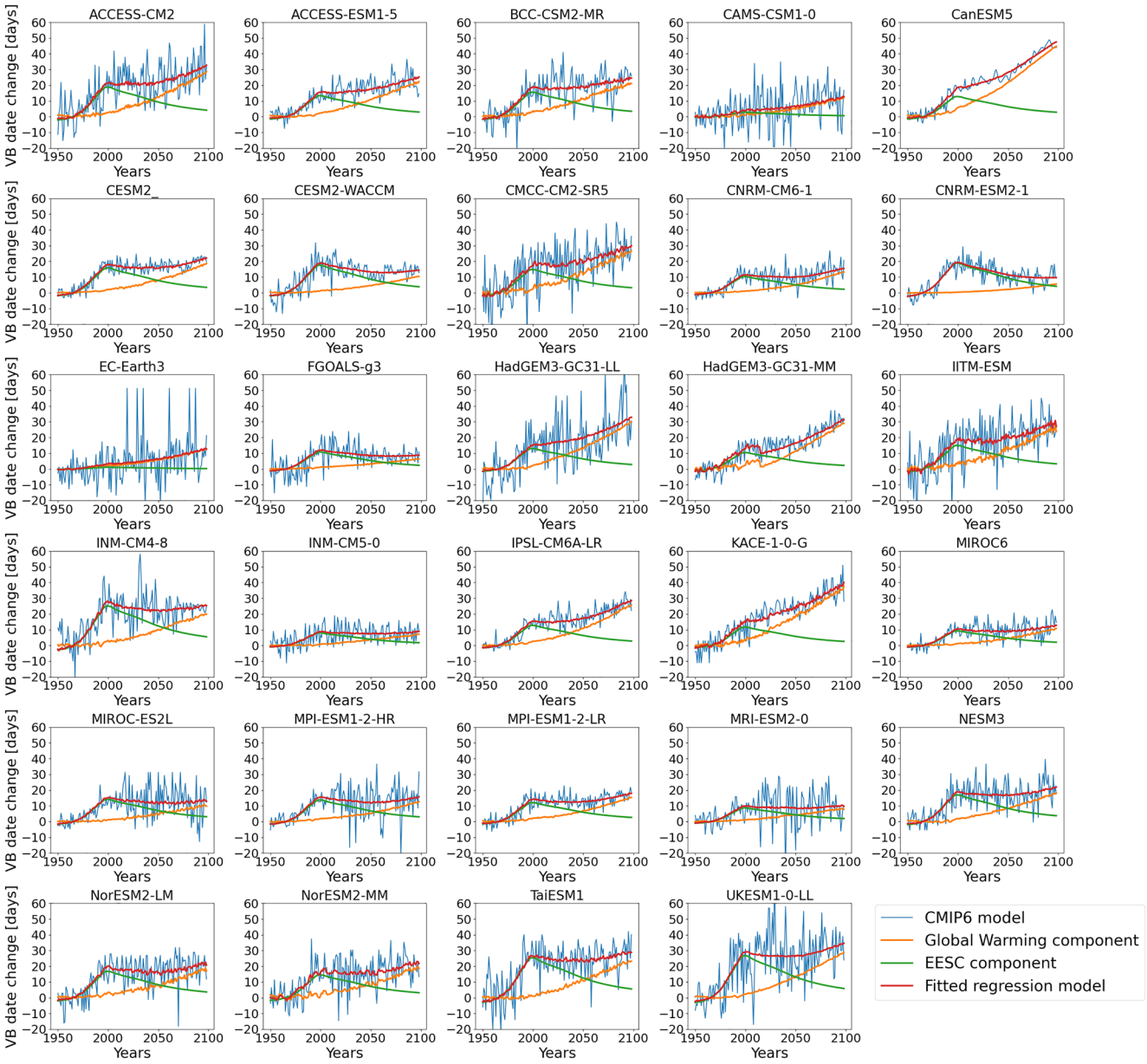

Figure 1. Each panel shows the ensemble mean VB date change with respect to the 1950–1969 climatology for an individual model (blue), the contributions of EESC (α_mEESC(t) in green) and GW (β_mGW$_m(t)$ in orange) to VB$_{delay}$ with (α_m, β_m) estimated for each model m with the linear regression model (Equation 1), and the total linear fit (red). EESC, equivalent effective stratospheric chlorine; GW, global warming; VB, vortex breakdown.

3. Combined Effects of GW and EESC on the Stratospheric Polar Vortex

We first consider the effect of ozone depletion and recovery together with that of GW on VB$_{delay}$ throughout the period 1950–2099 via the multiple linear regression model:

$$VB_{delay}(t) = \alpha\, EESC(t) + \beta\, GW(t) + \epsilon, \tag{1}$$

where ϵ is the residual. The result for each individual model is shown in Figure 1 and the response to the forcings is shown in Figure 2a. The obtained fits are excellent, implying that this parameterization represents the VB$_{delay}$ associated with these two forcings. The mean VB response to EESC (α) is 5 days ppb^{-1}; considering that from 1950 to 2000 the observed EESC increase was ~3 ppb, this shows that the CMIP6 ensemble captures the 2-week VB delay observed in the last decades of the 20th century (Langematz et al., 2003;

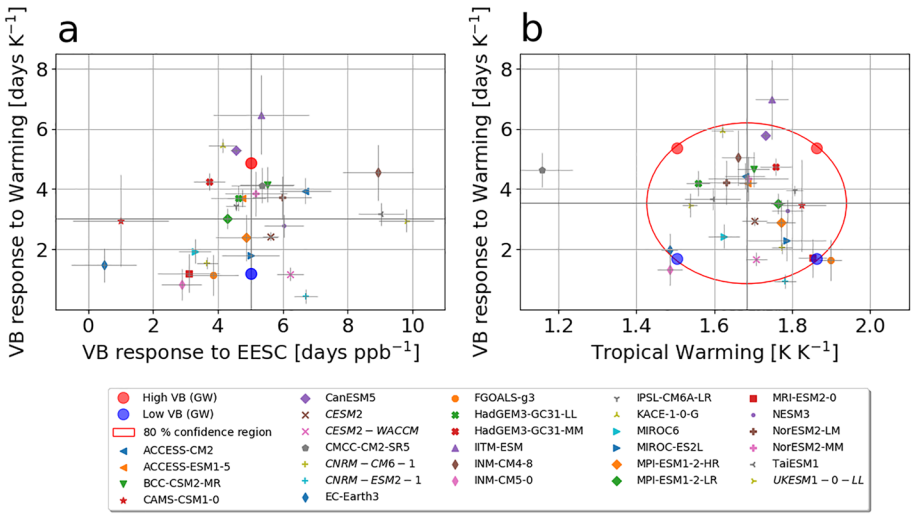

Figure 2. (a) Regression coefficients for VB response to EESC and GW from the time series analysis shown in Figure 1. The red and blue dots represent the storylines of high and low VB response to GW, respectively. The confidence intervals are estimated using a t-score two-tail test and the coefficients' standard error. (b) TW indices in DJF plotted against the VB response to GW (same indices as panel a), the red curve shows the 80% confidence ellipse of the joint χ^2 distribution with two degrees of freedom. Error bars for TW show the 95% confidence interval in the individual model responses of TW. The confidence intervals for TW are estimated, assuming white noise, from the year-to-year variability in the remote drivers, and also accounting for the number of ensemble members available for each model. The VB response to the GW storylines (red and blue dots in panel a) are expanded to four storylines when considering two plausible values of TW (panel b). Models with interactive ozone are indicated in italic font. EESC, equivalent effective stratospheric chlorine; GW, global warming; VB, vortex breakdown.

Previdi & Polvani, 2014; Waugh et al., 1999). Figure 1 shows that this feature is simulated by all models and is almost entirely explained by the EESC increase, with the exception of CAMS-CSM1-0 and EC-Earth 3for which the response to both forcings is very small (Figure 2a). For 70% of the models the VB_{delay} stabilizes after 2000 and remains roughly unchanged during 2000–2050 in which EESC diminishes and GW increases, reflecting a "tug-of-war" between the two effects. The mean VB response to GW (β) is 3.5 days K^{-1}, which means that for a warming of 3 K, the VB_{delay} is ~10 days. Almost half of the models show an above-average VB response to GW and therefore exhibit a continuing trend in VB_{delay} during the second half of the 21st century. The VB_{delay} in the rest of the models remains stable until the end of the century, but never returns to zero.

It has been recently shown that ozone-hole-induced summer circulation changes in the SH are well simulated by CMIP5 models (Son et al., 2018). Because of this, and the fact that the ozone fields produced for CMIP6 models without interactive chemistry are three-dimensional (Hegglin et al., 2016), we consider the CMIP6 ensemble fit for the purpose of this analysis. In addition, we find no systematic difference between the VB response to EESC in models with prescribed and interactive ozone (Figure 2a).

4. Combined Effects of Remote Drivers on Circulation and Precipitation

4.1. Storyline Definition and Evaluation

Figure 2a suggests that while the models' VB responds in a consistent way to EESC, with a few outliers, there is considerable spread in its response to GW. Thus, we now combine the spread in the VB response to GW with the spread in the long-term response of tropical upper-tropospheric temperature to GW, to articulate time-dependent storylines of circulation and precipitation change. The ensemble uncertainty in TW is shown together with the VB response to GW in Figure 2b. We choose to represent the effects of ozone depletion/recovery with a single storyline corresponding to the multimodel ensemble mean (MEM) VB_{delay} for simplicity and because it matches well the observed VB delay.

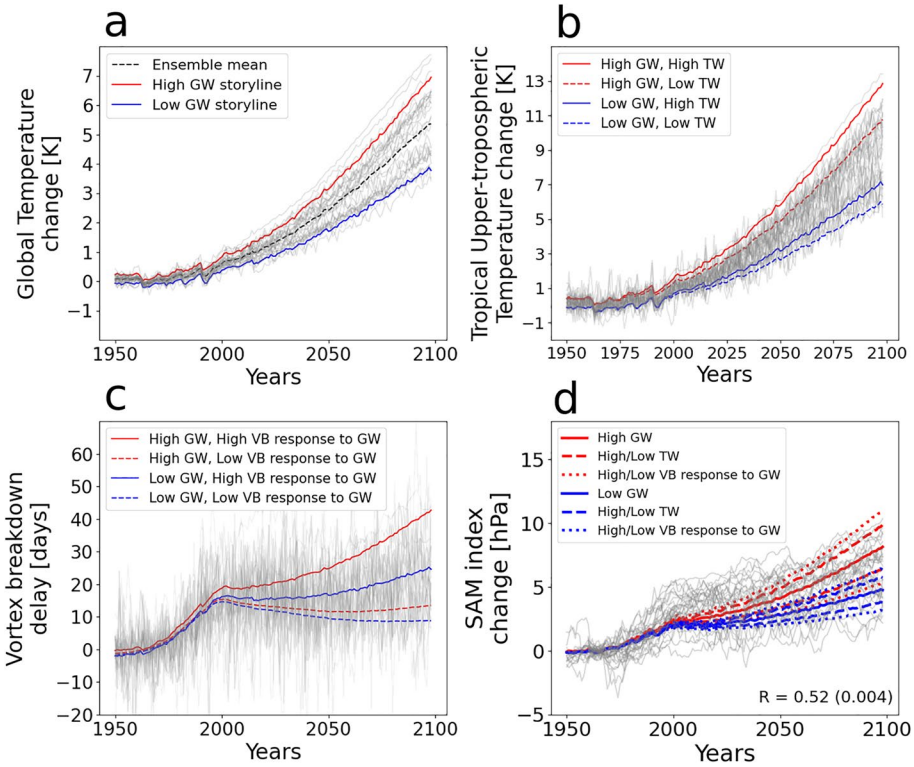

Figure 3. (a) GW with respect to the 1950–1969 climatology, the dashed line shows the MEM, the gray curves show the individual models' GW, the red and blue curves represent the storylines for high and low GW levels. (b) Tropical upper-tropospheric temperature change associated with the two GW storylines in (a), the solid and dashed lines are associated with the high and low TW storylines and gray lines show time-series of the individual models' ΔT_{trop}. (c) Same as panel (b) but for VB response to GW. (d) The SAM index anomaly spread associated with High/Low GW, and the High/Low TW and High/Low VB storylines. R is the Pearson correlation of the predicted SAM change estimated with the linear model against the individual model SAM changes, *p*-value in parenthesis. Gray lines are time-series of the individual models' SAM index change, for which a 10-year moving average is taken to remove year-to-year variability using the 1940–2099 period. GW, global warming; TW, tropical warming; VB, vortex breakdown; SAM, Southern Annular Mode.

In Figure 2, the red and blue dots show how we choose to span the space of model responses, parameterized by the two remote drivers' response to forcings. For the storylines to be physically plausible they are chosen to lie in the 80% confidence region of the joint distribution for the remote drivers (Zappa & Shepherd, 2017). The red dots correspond to a high VB response to GW ($\beta \sim 5.7$ days K^{-1}) and the blue dots to a low VB response ($\beta \sim 1.5$ days K^{-1}); only one storyline for the VB response to EESC ($\alpha \sim 5$ days ppb^{-1}) was investigated, which is why there are only two dots in Figure 2a. The double red and blue dots in Figure 2b show how we combined two extreme responses of TW ($\sim$1.5 KK^{-1} and $\sim$1.9 KK^{-1}) with the two storylines of VB response to GW in Figure 2a.

Because EESC evolves independently of GW (Figure 1) and we find an influence of EESC on the VB, the storylines cannot be expressed in terms of a warming level (Tebaldi & Arblaster, 2014) as in Zappa and Shepherd (2017) and Mindlin et al. (2020). Instead, we build in the time-dependence of both EESC and GW to define time-dependent storylines. Figure 3a shows that the warming level reached toward the end of the century in the SSP5-8.5 experiment is between 3 K-7.5 K, reflecting the spread in climate sensitivity. To account for this uncertainty together with that of the remote drivers, we articulate storylines for two warming levels (High/Low GW; Figure 3a). The two GW storylines were chosen to deviate 1.28 σ from the MEM GW; in this way, as with the remote driver storylines, they represent the 80% confidence region of the CMIP6 ensemble.

In Figure 3a the High/Low GW storylines are shown in red and blue respectively. Figure 3b shows, for each of the two GW storylines, what the tropical upper-tropospheric warming would be under a High/Low TW

Table 1
Area Average of DJF Precipitation Changes Per Degree of Warming (mm day^{-1} K^{-1}) Associated With the MEM, the Sensitivity of the Precipitation Field to Remote Driver Changes and the Four Storylines Shown in Figure 2b, Together With the MAD of the Residuals From the Statistical Model (Equation 2)*

Region	MEM	TW	VB to GW	VB to EESC*	Low TW Low VB	High TW Low VB	Low TW High VB	High TW High VB	Residual MAD
Extratropical Andes	−0.081	−0.038	0.007	−0.002	−0.042	−0.137	−0.024	−0.119	0.031
Southeastern South America	0.109	−0.031	0.001	0.003	0.146	0.068	0.149	0.071	0.033
East Coast of Australia	0.078	−0.023	0.008	0.006	0.090	0.034	0.121	0.063	0.042
New Zealand	0.046	−0.018	0.003	0.008	0.067	0.020	0.072	0.026	0.026
Tasmania	−0.056	−0.032	−0.007	−0.004	−0.006	−0.087	−0.024	−0.105	0.038
South East of South Africa	0.083	−0.030	0.043	0.001	0.063	−0.005	0.171	0.103	0.082

Note. Storyline changes are defined as the difference between the 2070–2099 and the 1991–2020 climatology.

Abbreviations: EESC, equivalent effective stratospheric chlorine; GW, global warming; MAD, medium absolute deviation; VB, Vortex breakdown.

*The sensitivity to TW and VB response to GW, expressed in units of mm day^{-1} K^{-1}, represents the sensitivity to one standard deviation in the remote drivers' response; the sensitivity to VB response to EESC, expressed in units of mm day^{-1} day^{-1}, represents the response to a day of VB delay.

storyline, together with the individual responses in the CMIP6 ensemble. In the same way, Figure 3c shows for each GW storyline the VB_{delay} that would occur under a High/Low VB storyline together with the individual responses in the CMIP6 ensemble. From Figures 3b and 3c, we conclude that the chosen storylines are able to represent the ensemble spread in the remote drivers throughout the entire period. We find that while the temperature change in the tropical upper troposphere is highly sensitive to the degree of warming (Figure 3b), in the stratosphere a low GW can still have a large effect on maintaining a delayed VB if the VB response to GW is high, while if the VB response to GW is low (Figure 3c), ozone recovery will drive an anticipation of the VB date during the 21st century regardless of the degree of warming. This sensitivity can be interpreted as a manifestation of the "tug-of-war" acting through the stratosphere, which depends on both the GW and the response of the VB to GW.

The slp and pr responses associated with these storylines are represented via:

$$\Delta C_{xi}(t) = (\hat{a}_x \pm \hat{b}_x TW_{80\%} \pm \hat{c}_x \beta_{80\%})\Delta T_i(t) + \hat{d}_x \overline{\alpha}\ \Delta EESC(t), \quad (2)$$

where ΔC_{xi} is the change in the field at grid point x for the high ($i = 1$) or low ($i = 2$) GW storylines. $\hat{a}_x$ is the MEM response to GW, $\hat{b}_x$, $\hat{c}_x$ and $\hat{d}_x$ are the sensitivities to the remote drivers evaluated with the regression framework, $TW_{80\%}$ and $\beta_{80\%}$ scale the responses of each remote driver to GW and $\overline{\alpha}$ is the MEM VB response to EESC. The four storylines are obtained with sign permutations. See SI for details.

4.2. Southern Annular Mode Under Time-Dependent Storylines

Panels a, b, and c in Figure 3 show storylines for GW, TW, and VB_{delay}, which represent the spread in the model responses by construction, as explained in Section 4.1. In Figure 3d we show the storyline spread in the time-dependent SAM index change. The storylines are seen to be able to well represent the spread in the model responses, which is a validation of the method. The Marshall SAM index is evaluated as the difference between the seasonal zonally averaged slp response at 40°S and 65°S as in Mindlin et al. (2020). We find that the slp changes per day of VB_{delay} south of 40°S are very similar between GW and EESC (see Figure S1), with the response to EESC forcing being more zonally symmetric. This suggests that the "tug-of-war" between ozone recovery and GW propagates from the stratosphere to the troposphere, helping to explain the flattening of the trend in the SAM index early in the 21st century and the strengthening of the trend toward the end of the century (Figure 3d). This further implies that the SAM response to GW not only depends on the warming level and other tropospheric mechanisms, but also on the VB response to GW.

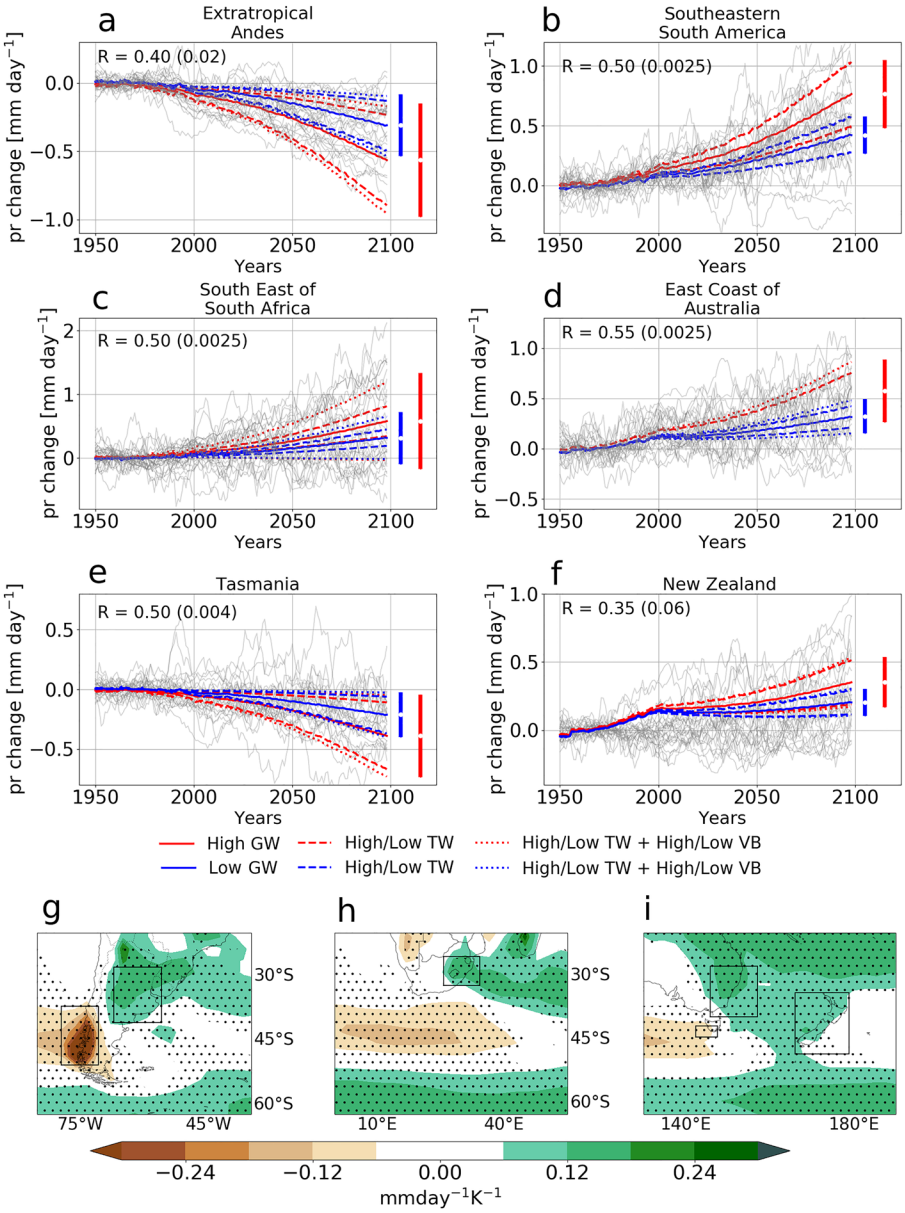

Figure 4. (a–f) Spread in the time-dependent storylines for DJF regional precipitation change over 1950–2099. The solid line represents the mean change for the High (red) and Low (blue) GW storylines, dashed lines show the spread between the High and Low TW storylines and dotted lines the spread between High and Low VB response to GW. The vertical bars on the right-hand side of each panel show the circulation-induced storyline spread in 2099 for each GW storyline. Gray lines show the regional precipitation change for the individual models, for which a 10-year moving average is taken using the 1940–2099 period. R is the Pearson correlation of the predicted regional precipitation change estimated with the linear model against the individual model precipitation changes, with *p*-values in parentheses. (g–i) MEM precipitation change and the regions for which the storylines are evaluated. Stippling indicates statistical significance, evaluated with a two-tail t-test with $\alpha = 0.05$. GW, global warming; TW, tropical warming; MAD, median absolute deviation; VB, vortex breakdown.

4.3. Regional Climate Changes Under Time-Dependent Storylines

Figures 4a–4f show the spread in the storylines of precipitation change averaged over the regional boxes in Figures 4g–4i, which correspond to inhabited land regions where the MEM shows statistically significant changes. In Table 1, we show the MEM change and the sensitivity to the remote drivers averaged over the regional boxes, the median absolute deviation (MAD) of the linear model residuals, and for each TW/VB

storyline, the end-of-century precipitation change per degree of warming with respect to recent climate (1991–2020, a period that covers the EESC peak and starts and ends with the same EESC levels). This is done by computing:

$$\Delta C_{\bar{x}} = \frac{\Delta C_{\bar{x}1} - \Delta C_{\bar{x}2}}{\Delta T_1 - \Delta T_2}, \quad (3)$$

where $\Delta C_{\bar{x}i}$ are the spatially averaged precipitation changes, for each TW/VB storyline, under the High and Low GW storylines evaluated with Equation 2. If the difference between the precipitation changes under two different TW/VB storylines is within the residuals' MAD, we consider the TW/VB storylines to be indistinguishable. In the two drying regions we find that the future drying is highly dependent on GW and TW, with the low GW/high TW storyline exceeding the high GW/low TW storyline (Figures 4a and 4e). However, the low VB response to GW would lead to a slightly drier storyline in Extratropical Andes, while in Tasmania this would occur for a High VB response to GW. Tasmania is the only region where a positive VB_{delay} leads to drying (Figure 1 and Table 1). In the wetting regions the highest impact is associated with High GW, Low TW and a High VB response to GW (Table 1), consistent with Mindlin et al. (2020). South East of South Africa is the only region that is highly sensitive to the VB response to GW, and New Zealand is the only region that is highly sensitive to ozone depletion. The overlap of the red and blue plumes in Figure 4, whose spread is indicated through the vertical bars on the right-hand side of each panel, shows that for regional end-of-century precipitation changes, the uncertainty in future circulation change is as important as the uncertainty in global warming level.

5. Conclusions

Changes in the late-spring/early summer stratospheric circulation throughout the period 1950–2099 have been explained by separating the response of the stratospheric polar vortex to ozone depleting substances and global warming. We showed that the "tug-of-war" between global warming and ozone recovery that occurs during the 21st century, driving respectively poleward and equatorward shifts in the tropospheric jet, takes place in the stratosphere and propagates to the troposphere, where it is combined with the effect of other remote drivers such as tropical upper-tropospheric warming.

Perhaps surprisingly, we found the role of the vortex breakdown response to EESC in driving regional precipitation changes to be generally small or even negligible. The one exception is New Zealand, but that is where our storylines have the least explanatory power. Instead, the tropical upper-tropospheric warming, and to a lesser extent the vortex breakdown delay associated with global warming, were found to be more relevant for representing the spread in Southern Hemisphere midlatitude regional precipitation changes. The lack of a strong role of EESC for summertime regional precipitation changes is not an artifact of our statistical analysis, as the individual model simulations in Figures 4a–4f do not suggest a time dependence that requires the use of EESC as an explanatory factor. However, the difference in the inferred regional precipitation response to GW-induced and EESC-induced VB changes suggests the presence of a missing driver in the analysis of the VB-precipitation connection, and warrants further investigation.

Data Availability Statement

All CMIP data are available from the ESGF at https://esgf-node.llnl.gov/projects/esgf-llnl/.

Acknowledgments
This study is supported by the ACRCC, ERC Advanced Grant 339390, the UBACyT project 20020130100489BA and the CLIMAX Project funded by Belmont Forum/ANR-15-JCL/-0002-01. J. Mindlin is supported by University of Buenos Aires. The authors thank both reviewers for their insightful comments.

References

Arblaster, J. M., & Meehl, G. A. (2006). Contributions of external forcings to southern annular mode trends. *Journal of Climate*, *19*, 2896–2905. https://doi.org/10.1175/JCLI3774.1

Ceppi, P., & Shepherd, T. G. (2019). The role of the stratospheric polar vortex for the Austral jet response to greenhouse gas forcing. *Geophysical Research Letters*, *46*, 6972–6979. https://doi.org/10.1029/2019GL082883

Eyring, V., Bony, S., Meehl, G. A., Senior, C. A., Stevens, B., Stouffer, R. J., & Taylor, K. E. (2016). Overview of the coupled model intercomparison project phase 6 (CMIP6) experimental design and organization. *Geoscientific Model Development*, *9*(5), 1937–1958. https://doi.org/10.5194/gmd-9-1937-2016

Gillett, N. P., & Thompson, D. W. (2003). Simulation of recent Southern Hemisphere climate change. *Science*, *302*(5643), 273–275. https://doi.org/10.1126/science.1087440

Hegglin, M., Kinnison, D., Lamarque, J.-F., & Plummer, D. (2016). CCMI ozone in support of CMIP6—Version 1.0. *Earth System Grid Federation*. https://doi.org/10.22033/ESGF/input4MIPs.1115

Kushner, P. J., Held, M., I., & Delworth, T. L. (2001). Southern Hemisphere atmospheric circulation response to global warming. *Journal of Climate*, *14*(10), 2238–2249. https://doi.org/10.1175/1520-0442(2001)014<0001:shacrt>2.0.co;2

Langematz, U., Kunze, M., Krüger, K., Labitzke, K., & Roff, G. L. (2003). Thermal and dynamical changes of the stratosphere since 1979 and their link to ozone and CO_2 changes. *Journal of Geophysical Research*, *108*(D1), https://doi.org/10.1029/2002jd002069

McLandress, C., Jonsson, A. I., Plummer, D. A., Reader, M. C., Scinocca, J. F., & Shepherd, T. G. (2010). Separating the dynamical effects of climate change and ozone depletion. Part I: Southern Hemisphere stratosphere. *Journal of Climate*, *23*, 5002–5020. https://doi.org/10.1175/2010JCLI3586.1

Mindlin, J., Shepherd, T. G., Vera, C. S., Osman, M., Zappa, G., Lee, R. W., & Hodges, K. I. (2020). Storyline description of Southern Hemisphere midlatitude circulation and precipitation response to greenhouse gas forcing. *Climate Dynamics*, *54*, 4399–4421. https://doi.org/10.1007/s00382-020-05234-1

Newman, P. A., Daniel, J. S., Waugh, D. W., & Nash, E. R. (2007). A new formulation of equivalent effective stratospheric chlorine (EESC). *Atmospheric Chemistry and Physics*, *7*, 4537–4552. https://doi.org/10.5194/acp-7-4537-2007

Previdi, M., & Polvani, L. M. (2014). Climate system response to stratospheric ozone depletion and recovery. *Quarterly Journal of the Royal Meteorological Society*, *140*, 2401–2419. https://doi.org/10.1002/qj.2330

Randel, W. J., & Wu, F. (1999). Cooling of the Arctic and Antarctic polar stratospheres due to ozone depletion. *Journal of Climate*, *12*, 1467–1479. https://doi.org/10.1175/1520-0442(1999)012<1467:cotaaa>2.0.co;2

Shepherd, T. G. (2019). Storyline approach to the construction of regional climate change information. *Proceedings of the Royal Society A: Mathematical, Physical and Engineering Sciences*, *475*(2225), 20190013. https://doi.org/10.1098/rspa.2019.0013

Son, S. W., Gerber, E. P., Perlwitz, J., Polvani, L. M., Gillett, N. P., Seo, K. H., et al. (2010). Impact of stratospheric ozone on southern hemisphere circulation change: A multimodel assessment. *Journal of Geophysical Research Atmospheres*, *115*, https://doi.org/10.1029/2010JD014271

Son, S.-W., Han, B.-R., Garfinkel, C. I., Kim, S.-Y., Park, R., Abraham, N. L., et al. (2018). Tropospheric jet response to Antarctic ozone depletion: An update with chemistry-climate model initiative (CCMI) models. *Environmental Research Letters*, *13*(5), 054024. https://doi.org/10.1088/1748-9326/aabf21

Stolarski, R. S., Douglass, A. R., Newman, P. A., Pawson, S., & Schoeberl, M. R. (2010). Relative contribution of greenhouse gases and ozone-depleting substances to temperature trends in the stratosphere: A chemistry-climate model study. *Journal of Climate*, *23*(1), 28–42. https://doi.org/10.1175/2009JCLI2955.1

Tebaldi, C., & Arblaster, J. M. (2014). Pattern scaling: Its strengths and limitations, and an update on the latest model simulations. *Climatic Change*, *122*, 459–471. https://doi.org/10.1007/s10584-013-1032-9

Thompson, D. W., & Solomon, S. (2002). Interpretation of recent Southern Hemisphere climate change. *Science*, *296*(5569), 895–899. https://doi.org/10.1126/science.1069270

Waugh, D. W., Randel, W. J., Pawson, S., Newman, P. A., & Nash, E. R. (1999). Persistence of the lower stratospheric polar vortices. *Journal of Geophysical Research*, *104*(D22), 27191–27201. https://doi.org/10.1029/1999JD900795

World Meteorological Organization. (2014). *Scientific Assessment of Ozone Depletion: 2014. Global Ozone Research and Monitoring Project-Report No. 55*.

Young, P. J., Butler, A. H., Calvo, N., Haimberger, L., Kushner, P. J., Marsh, D. R., et al. (2013). Agreement in late twentieth century southern hemisphere stratospheric temperature trends in observations and CCMVAL-2, CMIP3, and CMIP5 models. *Journal of Geophysical Research: Atmospheres*, *118*, 605–613. https://doi.org/10.1002/jgrd.50126

Zappa, G., & Shepherd, T. G. (2017). Storylines of atmospheric circulation change for European regional climate impact assessment. *Journal of Climate*, *30*, 6561–6577. https://doi.org/10.1175/JCLI-D-16-0807.1